eXPRESS Polymer Letters Vol.2, No.7 (2008) 461–473
Available online at www.expresspolymlett.com
DOI: 10.3144/expresspolymlett.2008.56

Multiple shape-memory behavior and thermal-mechanical properties of peroxide cross-linked blends of linear and short-chain branched polyethylenes

*I. S. Kolesov**, *H.-J. Radusch*

Martin Luther University Halle-Wittenberg, Center of Engineering Sciences, Chair Polymer Technology, D-06099 Halle (Saale), Germany

Received 12 March 2008; accepted in revised form 29 April 2008

Abstract. Thermally induced shape-memory effect (SME) in tensile mode was investigated in binary and ternary blends of two ethylene-1-octene copolymers with a degree of branching of 30 and 60 CH_3/1000C and/or nearly linear polyethylene cross-linked after melt mixing with 2 wt% of liquid peroxide 2,5-dimethyl-2,5-di-(tert.butylperoxy)-hexane at 190°C. The average cross-link density estimated by means of the *Mooney-Rivlin* equation on the basis of tensile test data was characterized between 130 and 170 mol·m^{-3} depending on the blend composition. Thermal analysis points out *multiple* crystallization and melting behavior of blends caused by the existence of several polyethylene crystal populations with different perfection, size and correspondingly different melting temperature of crystallites. That agrees well with the diversity of blends phase morphology characterized by atomic force microscopy. However, *triple*- and *quadruple*-SME could be observed only after two- and accordingly three-step programming of binary and tertiary blends, respectively, at suitable temperatures and strains. Compared to performances obtained for the same blend after single-step programming above the maximal melting temperature the significantly poorer characteristics of SME like strain fixity and strain recovery ratio as well as recovery strain rate occurred after multi-step programming.

Keywords: *smart polymers, shape-memory effect, polymer blends, polyolefins*

1. Introduction

Shape-memory (SM) polymers represent a specific class of smart polymers which can be advantageously used in several fields of application, e.g. cable and packaging industry [1, 2], medicine and automotive [3–6]. Preconditions for proper appearance of the thermally induced SM effect are the existence of a stable physical or covalent molecular network and glass or phase transition (melting), respectively, at convenient temperatures T_{trans} [4–6]. For covalent (e.g. peroxidic) cross-linked semicrystalline polymers a SM behavior with high performance can be achieved, if *firstly* the polymeric material shows sufficiently high strain at break as well as preferably lowest residual strain after unloading, and produces sufficiently high visco-elastic forces under load at programming temperature $T_{pr} > T_{trans}$. *Secondly*, its crystalline phase formed during cooling of the programmed (*loaded*) sample is able to fix efficiently the strain and visco-elastic forces stored in the network. The SM behavior is characterized by the response temperature, strain fixity and strain recovery ratios. The response temperature (T_{res}) corresponds to maximum of recovery strain rate $-d\varepsilon_r/dt$ in a linear heating run of a programmed and at low temperature (e.g. room temperature) unloaded specimen.

*Corresponding author, e-mail: igor.kolesov@iw.uni-halle.de

Strain fixity (R_f) and strain recovery ratios (R_r) are defined according to [4] by Equations (1):

$$R_f = \frac{\varepsilon_v}{\varepsilon_p}, \qquad R_r = \frac{\varepsilon_p - \varepsilon_{rec,m}}{\varepsilon_p} \tag{1}$$

where ε_p is the strain caused by programming, ε_v is the strain that remains after programming, cooling and unloading of specimen and $\varepsilon_{rec,m}$ is the residual strain that resides after thermal induced recovery (shrinkage) at maximum temperature of experiment.

The investigation of the SM effect of covalent cross-linked semicrystalline polymers and in particular of peroxidic cross-linked ethylene copolymers [7–10] showed a strong correlation between the melting temperature $T_m \equiv T_{trans}$ of the crystalline phase and the response temperature T_{res}, namely $T_{res} \approx T_m$. Thus, it may be assumed that the existence of several 'n' crystalline phases or/and crystal populations with different perfection, size and correspondingly with distinctly different melting temperatures $T_{m.i}$ in one polymeric material results presumably in a *multiple* SM behavior, i.e. in the appearance of the same or lower number of recovery strain $\varepsilon_{rec}(T)$ steps and accordingly $d\varepsilon_{rec}(T)/dt$ maxima with response temperatures $T_{res.i} \approx T_{m.i}$ where $1 \le i \le n$ (i is an even number).

The *triple*-shape memory behavior for two different complex polymer network systems which were prepared by photoinduced copolymerization of a methacrylate-monomer and poly(ε-caprolactone) dimethacrylate was already recently described by Bellin *et al*. [11]. These polymer network systems are formed from two types of chain sections/domains of different chemical constitution which connect network nodes and exhibit either melting process for both section/domain types or melting and glass transition, respectively, at two different temperatures. However, *triple*-shape memory effect appears only after programming in two-step process, i.e., at two temperatures agreeing with temperatures of melting or glass transition, whereas the suitable programming strains must be adjusted [11, 12]. Such polymeric materials with *multiple* SM behavior (*m*SMP) could certainly offer new interesting applications for SM polymers, e.g. intelligent fasteners, removable stents [11, 12], etc.

As is known (see e.g. [13]) the crystallinity, melting and crystallization temperature of polyethylenes and in particular of short-chain branched polyethylenes, e.g. ethylene-1-octene copolymers (EOC) decreases with increasing degree of branching. By means of blending of nearly linear high density polyethylene (HDPE) and EOCs with different 1-octene content and consequently different degree of branching the materials containing several crystalline phases with different $T_{m.i}$ and $T_{res.i}$ can be created. The multiple crystal populations can be created in polymer owing to multistep crystallization as it was shown by Varga *et al*. [14] for long-chain branched low-density polyethylene. The significant difference between the systems presented in this work and the network systems described by Bellin *et al*. [11, 12] are *firstly* the relatively chemical homogeneity of the links between network nodes which are predominantly ethylene sequences by reason that tertiary carbon atoms connected with branches are extra susceptible by peroxidic cross-linking [15] and *secondly* the low costs of polyethylenes and their processing. For above mentioned reasons, the objectives of the presented work were the production of peroxidic cross-linked binary and ternary blends on the basis of HDPE and two EOCs with medium and high degree of branching as well as the investigation on their SM behavior and their characterization by the relevant thermal and mechanical properties.

2. Experimental

2.1 Materials and processing

The polyethylenes used in this study are commercially available products (Dow Chemical, Schkopau, Germany), namely HDPE (KS 10100 UE) and metallocene-catalyzed homogeneous EOCs (AFFINITY™ PL 1280G and ENGAGE 8200) with approx. 30 and 60 hexyl branches per 1000 C (EOC30 and EOC60), respectively. In Table 1 few relevant parameters of these materials are given.

As cross-linking agent 2,5-dimethyl-2,5-di-(tert.butylperoxy)-hexane (DHBP) (Degussa Initiators GmbH & Co KG, Pullach, Germany) was employed. The use of DHBP resulted in a high efficiency and a good processability of the chosen systems due to the availability of two peroxy groups and the high thermal stability (up to 145°C) of DHBP as well as its fluidity at room temperature. The DHBP shows a better processability by cross-linking of EOCs compared to dicumyl peroxide

Table 1. Designations as well as some physical and molecular parameters of the used polyethylenes

Designation	Melt index (MI)* [dg/min]			Tm [°C]	Density [kg/m³]	Mass-average molecular mass $\overline{M}_w$ [kg/mol]	Polydispersity $\overline{M}_w/\overline{M}_n$	Degree of branching [CH_3 /1000C]
	190°C/ 2.16 kg	190°C/ 5.0 kg	130°C/ 5.0 kg					
HDPE	3.0	10.1	2.5	132	955	–	–	–
EOC30	5.0	17.7	4.2	96	900	64	2.3	~30
EOC60	4.4	15.9	3.4	59	870	87	2.5	~60

*detected by means of melt index test apparatus MI 21,6 (Göttfert Werkstoff-Prüfmaschinen GmbH, Buchen, Germany)

which entails gas release by cross-linking [9, 10]. Before blending the polymers were impregnated with DHBP. For these purposes the pellets of polymer were wetted with 2 wt% of DHBP and the fluid cross-linking agent was allowed to diffuse into these pellets placed in hermetic plastic flask for 3 days.

The mechanical mix of with DHBP impregnated polymer pellets in desired ratio (see Table 2) was then blended using a single-screw extruder (Brabender® GmbH & Co. KG, Duisburg, Germany) with the barrel temperature of 130°C whereby the distribution of DHBP was homogenized. As reference object a cross-linked HDPE was prepared and investigated in the same manner. It seems that homogenization of the peroxide in the melt-mixing process is essential for subsequent cross-linking. The processing experiments show that the applied cross-linking method is suitable for polyethylenes with the chosen melt index MI (see Table 1). At the same time, it should be noted that DHBP as a low-molecular substance can act as a lubricant at the processing temperature of 130°C in the extruder. Therefore the effective MI values of the DHBP impregnated polyethylenes are evidently higher and the viscosities are lower than that of pure materials. This effect supports the mixing process at 130°C. At higher temperatures immediately after the onset of the cross-linking process, the viscosity increases and the MI decreases dramatically with increasing temperature and duration of mixing. The extrudate was further processed to films with a thickness of 1 and 2 mm at 140°C and immediately cross-linked at a temperature of 190°C. The cross-linking time and temperature were optimized using a vulcameter Elastograph (Göttfert Werkstoff-Prüfmaschinen GmbH, Buchen, Germany).

2.2. Instrumentation

The *tensile tests* in the temperature range of SM tests programming (120 and 140°C) has been carried out using a testing machine Zwick 1425 (Zwick GmbH & Co. KG, Ulm, Germany) with heating chamber and a load cell 10 N at a crosshead speed of 50 mm/min after DIN EN ISO 527-1 (1996) standard. As specimens shouldered test bars were used with the cross-section area 2.0×2.0 mm^2 (test bar 5B according to DIN EN ISO 3167). The initial clamps distance was 20 mm.

Thermal analysis was performed with a heat-flux differential scanning calorimeter DSC 820 (Mettler-Toledo GmbH, Giessen, Germany) equipped with a ceramic sensor FRS5 and a liquid nitrogen cooling accessory. The heating and cooling scans were performed with 20 and 10 K/min, respectively.

Morphological investigations were carried out by an atomic force microscope Q-Scope 250 (Quesant

Table 2. Designations and composition of the extruded binary and ternary blends of polyethylenes used

Designation	Content of		
	HDPE [%]	EOC30 [%]	EOC60 [%]
100**HDPE**	100	–	–
50**HDPE**/50**EOC**30	50	50	–
33**HDPE**/33**EOC**30/34**EOC**60	33	33	34
10H**DPE**/45**EOC**30/45**EOC**60	10	45	45
10H**DPE**/25**EOC**30/65**EOC**60	10	25	65
50**EOC**30/50**EOC**60	–	50	50
30**EOC**30/70**EOC**60	–	30	70

Instrument Corporation, California, USA) operated in intermittent mode. Cantilever used are NSC 16 with resonance frequency f_R of 190 kHz and spring constant F of 48 N·m^{-1} (Nano and More GmbH, Wetzlar, Germany). Samples were produced by cutting in a cryo-chamber CN 30 (Microm-International-GmbH, Walldorf, Germany) with a diamond knife at –90°C.

For the characterization of the *shape memory behavior* the samples came at first under a specific temperature-deformation program. The samples were programmed by a stretching strain of $\varepsilon_{p1} \leq 100\%$ during a dwell period of 120 s at the programming temperature T_{p1}, and cooled down to T_{p2} with an average cooling rate of approx. 11 K/min in a constant deformed state. Before loading of the next programming strain ε_{pi} the sample temperature was kept constant for 10 min. After last programming step the specimen was cooled down to 10°C at the summary programming strain of 100%, thermal equilibrated for 10 min and unloaded. The recovery strain was measured first after a delay of 10 min at 25°C (ε_v) and than in the course of a heating run with a rate of 2 K/min and 'zero' stress of 70 Pa ($\varepsilon_{rec}(T)$). Complete SM investigations were carried out in tensile mode using a mechanical spectrometer measuring head Mark III (Rheometric Scientific Inc., New Jersey, USA).

3. Results and discussion

3.1. Uniaxial tension measurements. Cross-linking properties

The stress-strain diagrams of the investigated materials and their evaluation are depicted in Figure 1. The *Mooney-Rivlin* equation (2) for uniaxial tension (see [16, 17] and their references) was used for fitting the experimental results:

$$\sigma_{el} = 2C_1\left(\lambda - \frac{1}{\lambda^2}\right) + \frac{2C_2}{\lambda}\left(\lambda - \frac{1}{\lambda^2}\right) \qquad (2)$$

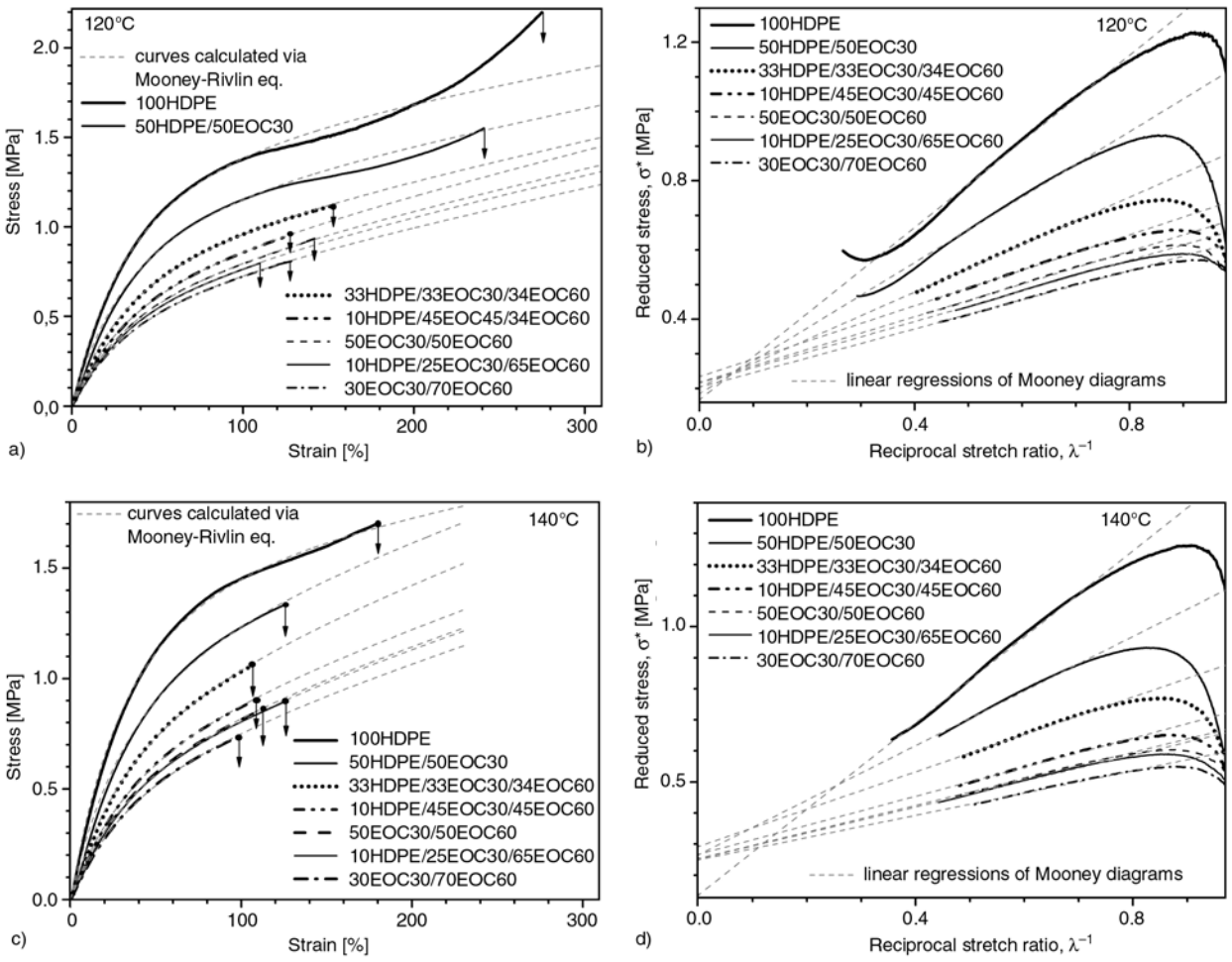

Figure 1. Stress-strain diagrams (a, c) and *Mooney* diagrams (b, d) of cross-linked HDPE and HDPE/EOC30/EOC60 blends at 120° (a, b) and 140°C (c, d) as well as their approximation on the basis of *Mooney-Rivlin* equation

where $2C_1$ is connected with shear *modulus G* and tensile *modulus E* as follows $2C_1 \equiv G = E/3$. The term $2C_1$ is responsible for the description of the influence of covalent network, the coefficient $2C_2$ takes into account entanglements, distribution of chain length, short-range order states and free chain tails.

Converting the *Mooney-Rivlin* equation (Equation (2)) a linear relationship between reduced stress $\sigma^* = \sigma_{el}/(\lambda - \lambda^{-2})$ and reciprocal stretch ratio λ^{-1} (Equation (3)) will be obtained:

$$\sigma^* = 2C_1 + \frac{2C_2}{\lambda} \tag{3}$$

In this connection the coefficients $2C_1$ and $2C_2$ of the *Mooney-Rivlin* equation were determined by means of linear regression of the corresponding legs of the *Mooney* diagram $\sigma^* = f(\lambda^{-1})$ as it is demonstrated in Figures 1b and 1d. The stress-strain diagrams which were generated on the basis of the obtained $2C_1$ and $2C_2$ coefficients agree quite well with the experimental results obtained for HDPE and HDPE/EOC30/EOC60 blends in the strain range till approx. 160% (see Figures 1a and 1c). However, HDPE and 50HDPE/50EOC30 blend at 120°C are exceptions in consequence of the still existing crystallites of HDPE.

According to the rubber elasticity theory [18] for a covalent network with a functionality of network nodes $f = 4$. Equation (4) follows for the *modulus E*:

$$E = \frac{3}{2}\nu_c \cdot R \cdot T = \frac{3\rho \cdot R \cdot T}{2\overline{M}_c} \tag{4}$$

where ν_c is the cross-link density, $R = 8.31$ kJ·(mol·K)$^{-1}$ is the gas constant, T is the absolute temperature, $\overline{M}_c$ is the average molar mass of the polymer chains between two neighboring network nodes and ρ is the density of polyethylene which amounts to 806 and 795 kg·m^{-3} [15, 19] at 120 and 140°C, respectively.

Thus, on the basis of Equations (2–4) the cross-link density and average molar mass of the polymer chains between two neighboring network nodes can be calculated by Equations (5):

$$\nu_c = \frac{2\cdot(2C_1)}{RT} \quad \text{and} \quad \overline{M}_c = \frac{\rho}{\nu_c} \tag{5}$$

The fitted values of the *Mooney-Rivlin* equation coefficients C_1 and C_2 as well as the calculated values of ν_c and $\overline{M}_c$ in combination with the experimentally determined values of strain at break ε_B and stress at break σ_B and stress at strain of 100% $\sigma_{100\%}$ of cross-linked HDPE and HDPE/EOC30/EOC60 blends are given in Table 3.

All investigated materials with the exception of HDPE (see Table 3) evidence a certain small increase of ν_c and consequently decrease of $\overline{M}_c$ values at higher temperature. The different behavior of HDPE is caused evidently by the above mentioned incomplete fusing of the crystalline HDPE

Table 3. Network parameters ν_c and $\overline{M}_c$ estimated from stress-strain diagrams on the basis of *Mooney-Rivlin* equation coefficients C_1 and C_2 as well as break strain ε_B and stress σ_B and stress at strain of 100% $\sigma_{100\%}$ of cross-linked HDPE and HDPE/EOC30/EOC60 blends

Blend composition	$2C_1$ [MPa]	$2C_2$ [MPa]	T [°C]	ν_c [mol/m^3]	$\overline{M}_W$ [kg/mol]	ε_B [%]	σ_B [MPa]	$\sigma_{100\%}$ [MPa]
100**HDPE**	0.168	1.244	120	103	7.860	275	2.20	1.38
	0.135	1.386	140	79	10.093	180	1.70	1.45
50**HDPE**/50**EOC**30	0.185	0.946	120	114	7.077	241	1.55	1.15
	0.266	0.879	140	155	5.140	126	1.33	1.23
33**HDPE**/33**EOC**30/34**EOC**60	0.204	0.685	120	125	6.456	125	1.12	0.96
	0.292	0.602	140	170	4.682	107	1.06	1.03
10**HDPE**/45**EOC**30/45**EOC**60	0.234	0.512	120	143	5.632	127	0.95	0.86
	0.267	0.468	140	155	5.119	109	0.91	0.87
50**EOC**30/50**EOC**60	0.218	0.473	120	133	6.049	142	0.93	0.79
	0.253	0.428	140	148	5.391	113	0.86	0.81
10**HDPE**/25**EOC**30/65**EOC**60	0.216	0.443	120	132	6.103	110	0.80	0.76
	0.252	0.418	140	147	5.419	126	0.90	0.81
30**EOC**30/70**EOC**60	0.203	0.421	120	125	6.455	128	0.81	0.72
	0.249	0.359	140	145	5.480	99	0.74	0.75

phase at 120°C. The ν_c values change insignificantly and vary approximately from 110 to 140 mol/m^3 at 120°C and from 80 mol/m^3 for HDPE as well as 150 to 170 mol/m^3 for blends at 140°C, respectively. Hereby the strain and stress at break as well as the stress at 100% strain (*E modulus* at high strain) increase with increasing HDPE content and as expected (see Equation (4)) with increasing temperature. Surprisingly, this increase does not correlate with the changes in cross-link density at least for HDPE and blends with high content of HDPE (50HDPE/50EOC30 and 33HDPE/33EOC30/34EOC60). For the explanation of this apparent discrepancy it should be mentioned that HDPE and blends with high HDPE content have explicitly higher crystallinity compared to blends with high content of branched polyethylenes (PE) whereas only the amorphous phase can be cross-linked as per definition. Correspondingly, if in high branched/low crystalline PEs the relatively homogenous distribution of network nodes may be expected, in high crystalline PEs the experimental determined (average) value of cross-link density differs dramatically from local cross-link density in presumably continuous amorphous phase. That entails a changed mechanical behavior of high crystalline PE materials in comparison with low crystalline PEs or PE blends at temperatures above melting temperature of blend components.

The values of strain at break from Table 3 point to the possibility of using a standard programming strain of 100% for investigation of shape memory behavior in present materials since the ε_B values of almost all investigated materials higher than or nearly equal to100%.

3.2. Melting and crystallization behavior

The melting and crystallization behavior of HDPE and HDPE/EOC30/EOC60 blends is displayed in Figure 2. First heating runs for all examined blends exhibit a minimum followed by a maximum in the temperature range between approx. 0 and 70°C caused by annealing at room temperature during storage of prepared samples, as it was shown for uncross-linked EOCs especially with high degree of branching [20]. Since, this phenomenon complicates melting thermograms which are already complex enough, only second heating runs were used for detailed analysis of melting behavior. Second

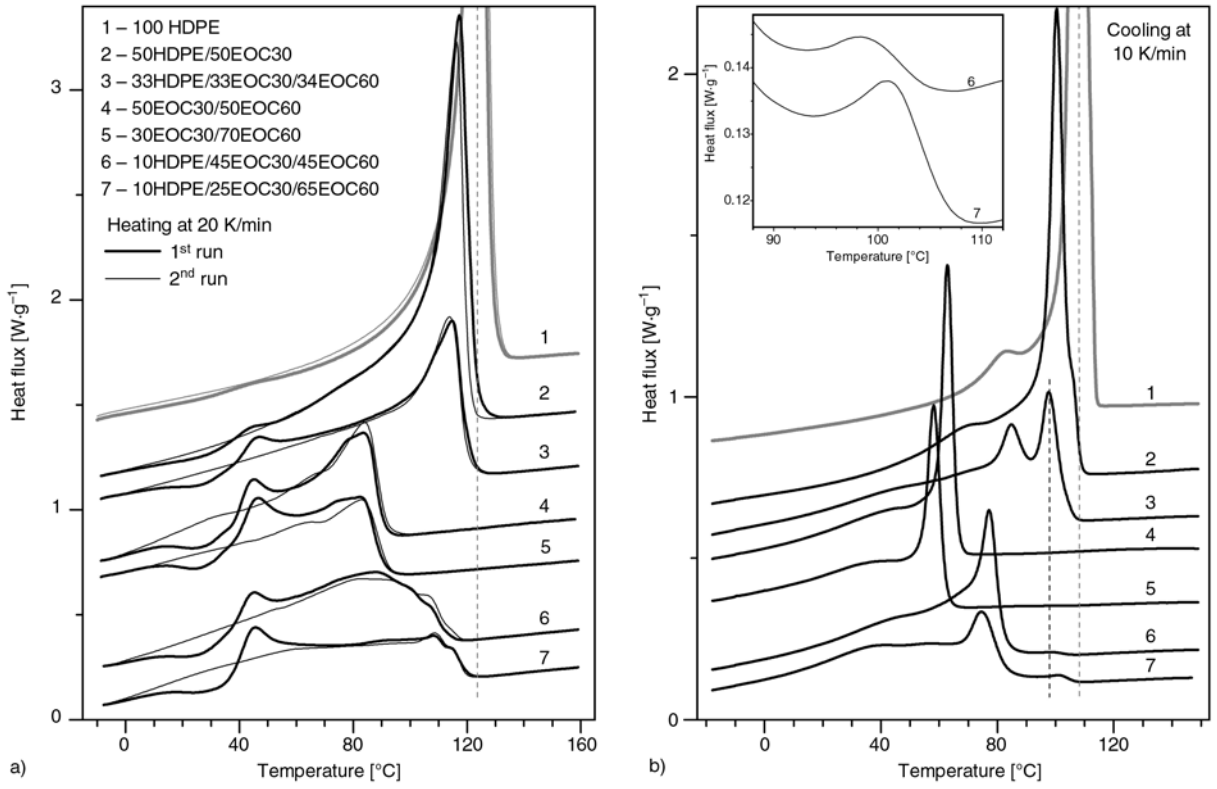

Figure 2. Melting (a) and crystallization (b) DSC thermograms of cross-linked HDPE and HDPE/EOC30/EOC60 blends. The 1st and 2nd heating runs (a) show a melting behavior of specimens stored after preparation for a long time at room temperature and after crystallization at cooling rate of 10 K/min, respectively

Table 4. Melting (T_{m}HDPE, T_{m}EOC30 and T_{m}EOC60) and crystallization temperatures (T_{c}HDPE, T_{c}EOC30 and T_{m}EOC60) of HDPE, EOC30 and EOC60 phases and total melting ($\Delta H_{m\Sigma}$) and crystallization enthalpy ($\Delta H_{c\Sigma}$) of HDPE/EOC30/EOC60 blends, respectively, as well as crystallization enthalpy of HDPE phase (ΔH_{c}HDPE) depending on blend composition

Blend composition	Melting				Crystallization				
	T_{m}HDPE [°C]	T_{m}EOC30 [°C]	T_{m}EOC60 [°C]	$\Delta H_{m\Sigma}$ [kJ/kg]	T_{c}HDPE [°C]	T_{c}EOC30 [°C]	T_{c}EOC60 [°C]	$\Delta H_{c\Sigma}$ [kJ/kg]	ΔH_{c}HDPE [kJ/kg]
100**HDPE**	124.3	–	–	139	108.0	–	–	139	139
50**HDPE**/ 50**EOC**30	116.1	[1]	[1]	108	100.3	~71	–	109	~75
33**HDPE**/ 33**EOC**30/ 34**EOC**30	114.0	[1]	[1]	86	97.7	84.7	~20[2]	89	~20
50**EOC**30/ 50**EOC**60	–	85.0	~68[2] ~35[2]	68	–	62.8	~46[3]	68	–
30**EOC**30/ 70**EOC**60	–	82.7	64.7 ~35[2]	64	–	58.2	~39[3]	63	–
10**HDPE**/ 45**EOC**30/ 45**EOC**60	~114[2] ~105[3]	~91[3] 82.9	~53[2]	74	97.7	77.2	~45[3]	73	~0.7
10**HDPE**/ 25**EOC**30/ 65**EOC**60	~115[3] 108.3	~94[2] ~79[2]	~61[3] ~30[2]	65	100.3	74.3	55.7 40.3	68	~1.5

[1]the peaks or shoulder which are assignable to EOC30 or EOC60 phase were not found in the thermogram;
[2]weak and flat shoulder;
[3]distinct shoulder

heating runs are recorded after crystallization at a cooling rate of 10 K/min and with short dwell time at lowest temperature of the experiment what agrees well with measuring conditions in SM experiments described beneath.

Generally, as illustrated in Figure 2 and Table 4 all blends, especially ternary blends demonstrate *multiple* behavior for both melting and crystallization. In 10HDPE/45EOC30/45EOC60 and 10HDPE/25EOC30/65EOC60 blends the HDPE phase crystallizes not only at 97.7 and 100.3°C, respectively, because the crystallization enthalpy estimated on the basis of these small peaks, which are depicted with high resolution in insert of Figure 2a, amounts to just approx. 5 and 10% of the expected value, respectively, (see Table 4; cp. with ΔH_{c} value of 'bulk' cross-linked HDPE). The ΔH_{c}HDPE value of 33HDPE/33EOC30/34EOC60 blend is at least two times lower than expected. These differences between real and expected ΔH_{c}HDPE values cannot be satisfactory explained on the basis of the difference in cross-link density between HDPE and blends (see Table 3) due to the fact that at 'pure' EOC30 the doubling of cross-link density results in a crystallinity decrease of only 1 to 3% at 25°C depending on the thermal history of specimen [10]. Moreover, the local cross-link density in the HDPE phase is by all means lower than the average cross-link density of the blend as a whole as given in Table 3. Obviously, the described behavior of blends suggests the crystallization of the main part of HDPE phase together with the EOC30 phase (or some part of it) at significantly lower temperature. Interestingly, the melting of the HDPE phase in 10HDPE/45EOC30/ 45EOC60 and 10HDPE/25EOC30/65EOC60 blends occurs also stepwise in two stages (see Figure 2a, curves 6 and 7).

The melting (T_{m}) and crystallization temperature (T_{c}) of the HDPE phase decrease markedly with decreasing HDPE content in the blend compared to the values for 'bulk' cross-linked HDPE. At the same time, T_{m} and T_{c} values of the EOC30 phase can increase in blends containing HDPE or decrease in binary blends with high branched EOC60 (see Table 4; cp. with T_{m} values of approx. 91 and 57°C for 'pure' EOC30 and EOC60, respectively, having a similar cross-link density).

If the increase of T_{c}EOC30 and correspondingly T_{m}EOC30 values can be explained as a result of the nucleating effect of existing HDPE crystallites in the cooling run, both the decrease of T_{c} and T_{m} values of HDPE and EOC30 phases as well as a *multi-*

ple melting and fractionated crystallization behavior points indirectly at significant molecular interaction of blend components in molten state but solely in regions where the molecular level of mixing before cross-linking was achieved. In blends both the nucleating effect of HDPE crystallites and molecular interaction are available only in *un*cross-linked crystalline domains which consist of ethylene sequences of blend components with suitable length. The cross-linking fixes partly the content, number and size of these domains but their perfection and structure can be changed depending on thermal history.

Due to the existence of several populations of PE crystallites of different stability and correspondingly with different melting temperatures in the described blends the thermograms in Figure 2a show nearly continuous melting that stretches across a very wide temperature range by what the macroscopic thermal-mechanical and in particular SM behavior of these blends (see section 3.4) is affected.

It should be noted that the total melting and crystallization enthalpy of blends decrease as expected with decreasing content of components with higher ability to crystallization (HDPE and EOC30).

3.3. Phase morphology

Mode and mechanism of phase morphology formation in present blends differ considerably from the behavior that demonstrate conventional polymer blends *firstly* due to high affinity of components which all are basically polyethylenes with degree of branching of approx. 0, 30 and 60 CH_3/1000C and with close-by values of MI/melt viscosity and *secondly* in consequence of melt structure and its fixation and of crystallization restrictions caused by cross-linking.

The lamellae or some part of them can be a part of chain sections which serve as links between network nodes. Alternatively, the crystallites (e.g. lamellae or their agglomerates) may be bound by links, namely unordered chain sections which form covalent network nodes on the crystallite surface. Obviously, both mechanisms take place but within the framework of present work it is not possible to establish which kind of links dominates and is more related to shape-memory properties.

Phase separation in amorphous regions takes definitely place already in molten state before the start of cross-linking and is evidently caused by the different average degree of branching of the blend partners [21] and the inhomogeneous distribution of branches between and along the molecular chains. According to [21] the linear HDPE and EOC30 should be miscible on the molecular level at temperatures ≥150°C. In contrast, the blend of HDPE and EOC60 cannot exhibit miscibility at processing temperatures. In branchless domains of sufficiently wide meshed network the molecular chains can be ordered in the course of cooling, but the crystallization must be pronounced restricted due to the melt structure and its fixation as a result of cross-linking. Thus, some part of crystallites can arise due to *co*-crystallization of suitable ethylene sequences of HDPE and EOCs whereon the crystallization behavior indirectly points (see section 3.2). At the same time, each blend component can also crystallize separately. Consequently the formation of multiple crystal populations of different size/stability and perfection may be expected.

In this connection the AFM images (Figure 3) demonstrate such a wide variety of morphology elements. In addition to certain number of dispersed particles the AFM images show a tendency to the formation of continuous phases which are however inhomogeneous, i.e., they include both amorphous and crystalline parts. The phase morphology of 50HDPE/50EOC30 and 33HDPE/33EOC30/34EOC60 blends (see Figure 3a and 3b), in which multiple shape-memory effect appears most pronounced (see section 3.4), exhibits distinct trend to the formation of nearby continuous extended macro domains integrated into the matrix that consists presumably of crystallites as e.g. lamellae and 'small' amorphous regions with a size of less than 100 nm. It seems that 'big' amorphous domains of approximately 150 and 500 nm in size for 50HDPE/50EOC30 and 33HDPE/33EOC30/34EOC60 blends, respectively, are enclosed into the 'crystalline' matrix. Lower differences in the degree of branching between the components and the smaller average degree of branching of 50HDPE/50EOC30 compared to other blends result in explicitly finer phase morphology with more pronounced separation of crystalline and amorphous phases. Here, it should be noted that enclosed 'big'

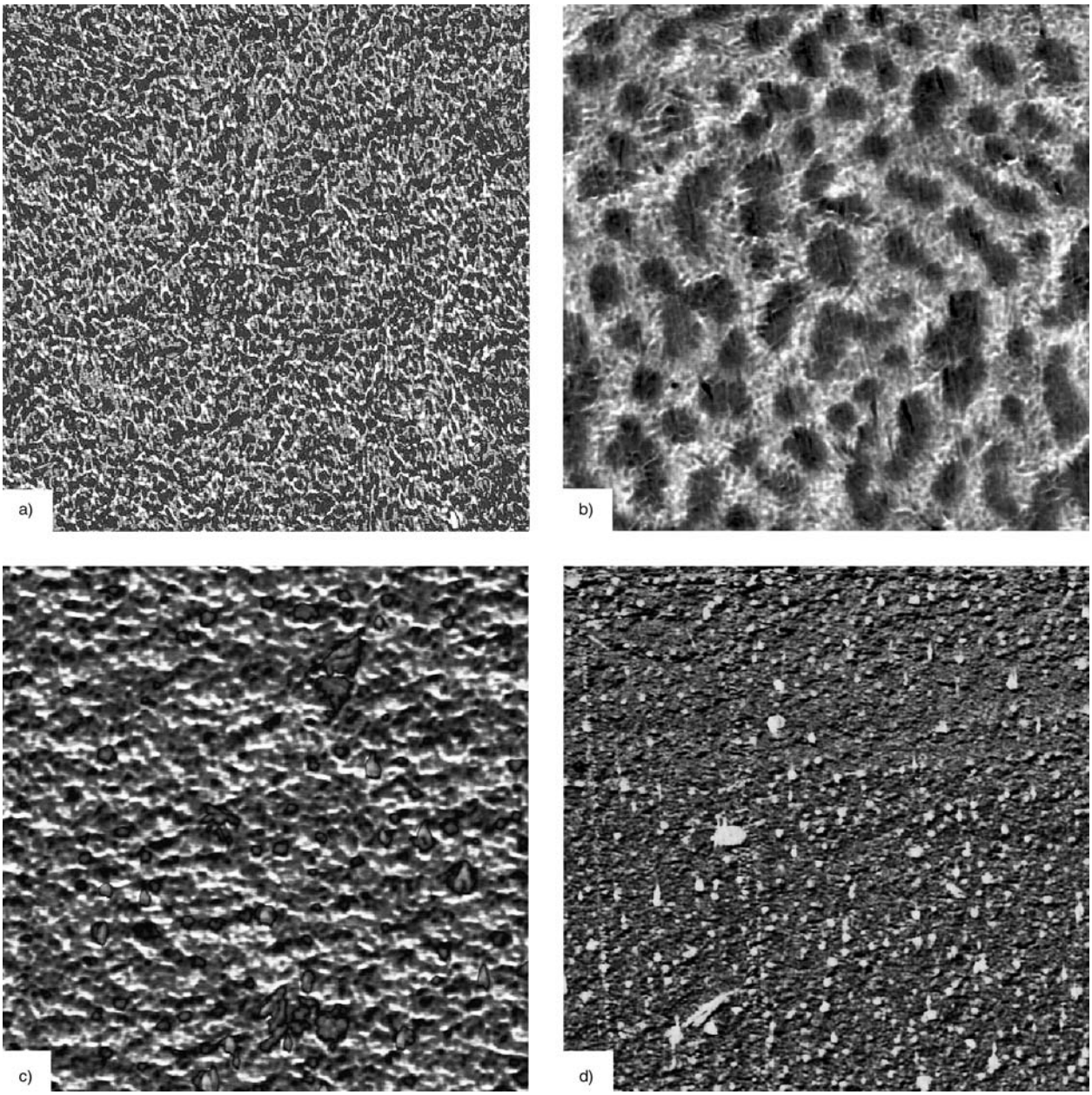

Figure 3. AFM phase images of 50HDPE/50EOC30 (a), 33HDPE/33EOC30/34EOC60 (b) and 10HDPE/25EOC30/65EOC60 blends (c and d) with size of 5×5 μm^2

amorphous domains in the 33HDPE/33EOC30/34EOC60 blend appear some softer in harder regions which are accordingly less or more ordered. In other blends, e.g. in 10HDPE/25EOC30/65EOC60, significant differences in the phase morphology of various regions exist that can be caused by an insufficient mixing quality in the single screw extruder and/or by the decomposition following processing before cross-linking. Two representative images in Figure 3c and 3d demonstrate the relatively fine smooth phase structure with a size of approx. 50 to 150 nm and sharp segregated nearly spherical hard particles assumedly of HDPE with a size of approx. 30 to 300 nm (Figure 3d), respectively.

3.4. Shape-memory behavior

The temperature dependence of SM recovery strain and recovery strain rate of HDPE and HDPE/EOC30/EOC60 blends and their components having a network with similar cross-link density are demonstrated in Figure 4. Here, the findings of the first cycle of SM tests are demonstrated. The results evaluating these curves are presented in Table 5.

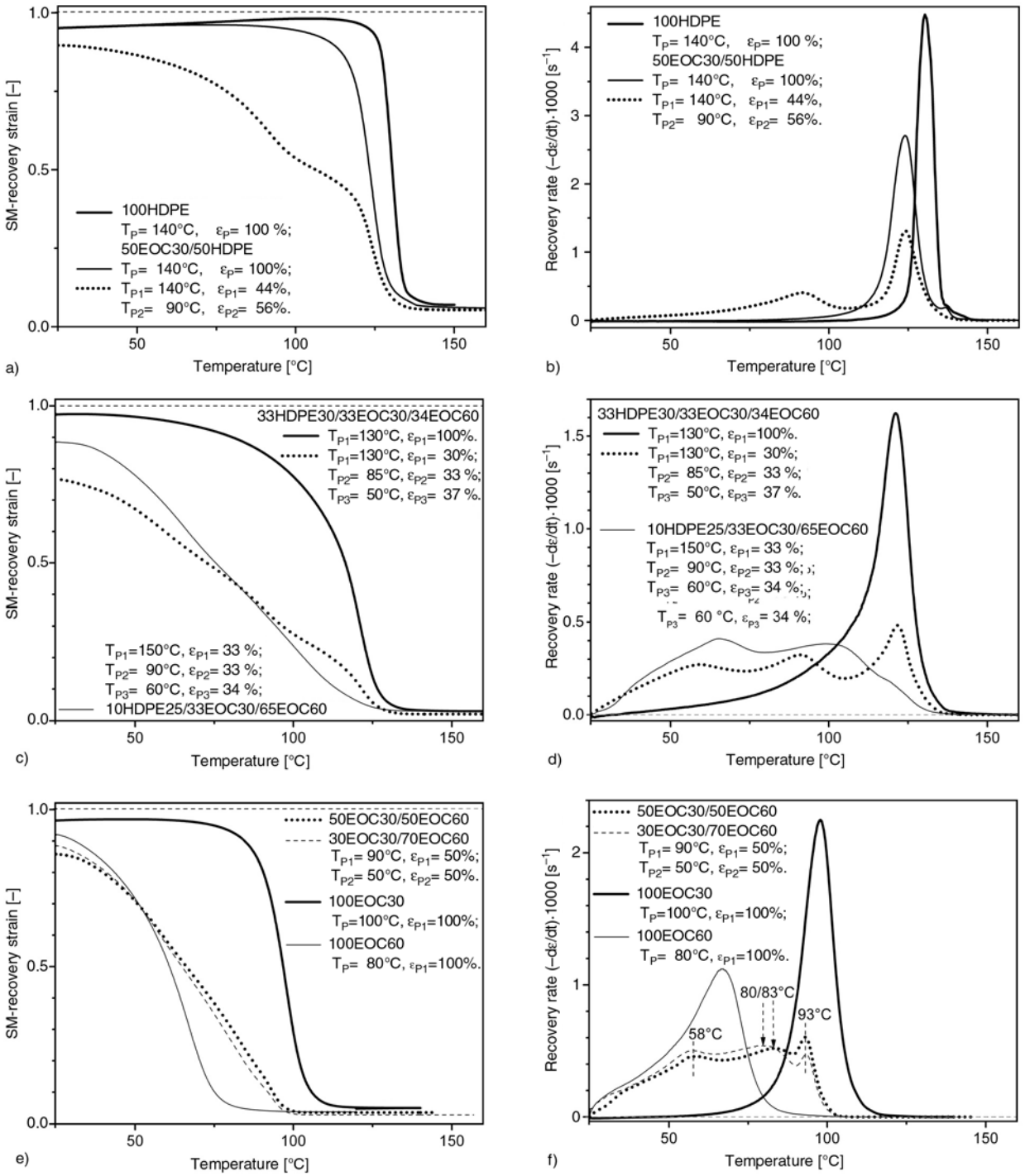

Figure 4. Effect of composition and programming conditions on the temperature dependence of SM recovery strain (a, c and e) and recovery strain rate (b, d and f) of HDPE and HDPE/EOC30/EOC60 blends

The sharp step of SM recovery strain and high, well separated peaks of SM recovery rate can be generated only by melting of a phase with sufficient crystallinity and relatively perfect crystallites which produce strong and well separated DSC peaks. For the explicit appearance of SME the availability of stored sufficiently high visco-elastic forces is important no less than suitable melting behavior. These visco-elastic forces caused by network deformation during programming must be efficiently stored by the crystalline structure formed in the actual temperature range, i.e. the crystalline structure must hold the reached deformation after unloading.

As expected, the blends having a higher average crystallinity which exhibit the distinct well

Table 5. Shape memory characteristics of HDPE, EOC30 and EOC60 phases and their blends including strain fixing (R_f) and strain recovery ratios (R_r), response temperature T_{res} as well as peak value of SM recovery rate $[-d\varepsilon/dt]_{max}$

Composition	R_f [%]	R_r [%]	T_{res} [°C]			$[-d\varepsilon/dt]_{max} \cdot 10^3$ [s^{-1}]		
			1	2	3	1	2	3
100**HDPE**	95.0	93.0	130.3	x	x	4.47	x	x
50**HDPE**/ 50**EOC**30	95.0	94.0	124.1	x	x	2.71	x	x
	90.0	95.0	124.1	91.8	x	1.32	0.41	x
33**HDPE**/ 33**EOC**30/ 34**EOC**30	97.0	97.0	121.1	x	x	1.62	x	x
	76.7	98.0	121.7	91.0	59.2	0.48	0.33	0.27
10**HDPE**/ 25**EOC**30/ 65**EOC**60	88.5	97.0	~120*	98.8	65.6	0.17	0.38	0.41
100**EOC**30	96.8	95.0	97.6	x	x	2.25	x	x
50**EOC**30/ 50**EOC**60	85.8	96.0	58.3	83.0	93.1	0.46	0.52	0.60
30**EOC**30/ 70**EOC**60	85.8	97.0	57.5	80.0	93.3	0.51	0.54	0.47
100**EOC**60	108.3	96.0	66.9	x	x	1.12	x	x

*shoulder which is assignable to the HDPE phase was not found in the DSC thermogram

resolved melting peaks exhibit the high strain fixity ratio R_f and SM recovery rate $-d\varepsilon_{rec}/dt$. Correspondingly, these parameters increase with increasing HDPE (and partly EOC30) content in the blends. The *single*-step programming of all blend types results in appearance of only one step and accordingly one peak in the temperature dependences of the SM recovery strain and SM recovery rate, respectively, i.e. in *dual*-shape behavior. It should be noted that these programming experiments were carried out at a temperature higher than the melting temperature of HDPE or EOC30 (depending on blend composition), i.e. at temperature at which entire blend is kept in molten state. Compared to the specimens arranged by means of *single*-step programming the same blends after *two*- or *three*-step programming show significantly lower R_f and $-d\varepsilon_{rec}/dt$ values and particularly $[-d\varepsilon_{rec}/dt]_{max}$ values at melting temperatures of the components (see Figure 4 and Table 5). The decrease of R_f values as a result of multi-step programming is caused by the partial deformation of already crystallized (fixed) phase/phases by each next programming step at lower temperature. These strain components are not fixed due to subsequent crystallization at lower programming temperature and are predominantly reversible at low temperature. The temperatures for *two*- or *three*-step programming were chosen allowing for the temperatures of a quiescent crystallization of present crystal populations obtained by means of DSC. Obviously, however a potential strain-induced crystallization should be taken into account. Perhaps the multi-shape behavior can be improved on the basis of further optimization of both programming temperatures and dwell periods. For this purpose, due to the possibility of partly strain-induced crystallization by programming [11, 12] the crystallization temperatures of blend components must be stated more precisely under load. The long-term stress relaxation experiments at programming temperatures and then subsequently SM recovery tests are necessary in order to reduce as much as possible the non-stored component of visco-elastic forces by means of suitable increasing of programming period, respectively. The last declaration hypothesizes that in already crystallized phase/crystal populations the structure changes connected with partial transformation of elastic and visco-elastic deformation of network to plastic deformation of existing crystalline phase can take place and are in need of more time as dwell period used in present work (120 s). Furthermore, with decreasing programming temperature the decrease of diffusion velocity of yet moveable chains is due. In this connection the better fixing of intermediate shape due to more completed isothermal and strain induced crystallization and presumptive creep of existing crystalline formations at longer programming dwell can be expected.

All investigated blends and their components independent from programming mode demonstrate rel-

atively high values of strain recovery ratio (R_r) that amounts approx. 93 to 98%.

Presumably, the *multi*-shape behavior by *single*-step programming may be carried out only in a heterogeneous polymer material having hypothetical phase morphology with preferred orientation of planar phase layers perpendicularly to load direction. However, if the same heterogeneous polymer material will be loaded parallel to planar phase layers the *multi*-shape behavior would be basically impossible because the specimen length in recovery stage can substantial change only after melting in layer with highest melting temperature starts. Thus, the important disadvantage of such hypothetical heterogeneous polymer material would be total anisotropy and as a consequence the inability to *multi*-shape behavior by programming load in two perpendicular directions what is important for some applications [11, 12].

4. Conclusions

Tensile test at 120 and 140°C *firstly* has permitted the evaluation of average cross-link density of blends that amounts approx. 110÷170 mol·m^{-3} depending on content and temperature, *secondly* has shown that by default used programming strain of 100% is acceptable for all blends, *thirdly* pointed at an increase of programming stress at strain of 100% and correspondingly of stored visco-elastic forces with increasing in blend part of components with higher crystallinity (EOC30 and predominantly HDPE).

The finding of the investigation of EOC/HDPE blends show that multiple SM behavior appears only at consequent stepwise application of convenient programming strains and temperatures. However, only for 50HDPE/50EOC30 blend which shows especially fine disperse and distinctly segregated phase morphology the temperature dependence of SM recovery strain demonstrates two pronounced steps. All other binary and tertiary EOC/HDPE blends exhibit the *triple*- and *quadruple*-shape-memory effect, respectively, only as very diffuse steps in SM recovery strain curves and as small, superimposed peaks of SM recovery rate vs. temperature. Obviously, that is caused by multiple melting behavior of these blends with many poorly separated peaks.

In spite of described problems the present blends have a good potential for further development and successful application. It should be also noted that some applications could be in need of gradual changes of sample geometry with low thermal-induced recovery strain rate. In the investigations the blends will be prepared with different degree of component dispersion as well as blends having a uncross-linked crystallizable disperse phase/phases.

Acknowledgements

The authors gratefully acknowledge the financial support by Deutsche Forschungsgemeinschaft (DFG). Samples of DHBP peroxide were kindly provided by Degussa Peroxygen Chemicals, Degussa Initiators GmbH & Co KG (Germany).

References

[1] Ota S.: Current status of irradiated heat-shrinkable tubing in Japan. Radiation Physics and Chemistry, **18**, 81–87 (1981).

[2] Kleinheins G., Starkl W., Nuffer K.: Besonderheiten bei der Qualitätssicherung strahlungsvernetzter Wärmeschrumpferzeugnisse. Kunststoffe, **74**, 445–449 (1984).

[3] Lendlein A., Langer R.: Biodegradable, elastic shape-memory polymers for potential biomedical applications. Science, **296**, 1673–1676 (2002).

[4] Lendlein A., Kelch S.: Shape-memory polymers. Angewandte Chemie, International Edition, **41**, 2034–2057 (2002).

[5] Behl M., Lendlein A.: Actively moving polymers. Soft Matter, **3**, 58–67 (2007).

[6] Ratna D., Karger-Kocsis J.: Recent advances in shape memory polymers and composites: A review. Journal of Materials Science, **43**, 254–269 (2008).

[7] Li F., Chen Y., Zhu W., Zhang X., Xu M.: Shape memory effect of polyethylene/nylon 6 graft copolymers. Polymer, **39**, 6929–6934 (1998).

[8] Li F., Zhu W., Zhang X., Zhao C., Xu M.: Shape memory effect of ethylene-vinyl acetate copolymers. Journal of Applied Polymer Science, **71**, 1063–1070 (1999).

[9] Kolesov I. S., Radusch H.-J.: Formgedächtnis in vernetzten Ethylen-1-Octen-Copolymeren. in: 'Proceedings of '11. International Conference Polymeric Materials 2004. Halle/Saale, Germany' PII–50 (2004).

[10] Kolesov I. S., Androsch R., Radusch H.-J.: Thermal-mechanical stability of covalent network and shape memory effect in ethylene-1-octene copolymers cross-linked by peroxides. in 'CD Proceeding of PPS-23 – The Polymer Processing Society 23rd Annual Meeting 2007. San Salvador, Brazil' P11-005, 1–6 (2007).

[11] Bellin I., Kelch S., Langer R., Lendlein A.: Polymeric triple-shape materials. Proceedings of the National Academy of Science of the USA, **103**, 18043–18047 (2007).

[12] Bellin I., Kelch S., Lendlein A.: Dual-shape properties of triple-shape polymer networks with crystallisable network segments and grafted side chains. Journal of Materials Chemistry, **17**, 2885–2891 (2007).

[13] Bensason S., Minick J., Moet A., Chum S., Hiltner A., Baer E.: Classification of homogeneous ethylene-octene copolymers based on comonomer content. Journal of Polymer Science: Part B, Polymer Physics, **34**, 1301–1315 (1996).

[14] Varga J., Menczel J., Solti A.: Memory effect of low-density polyethylene crystallized in a stepwise manner. Journal of Thermal Analysis and Calorymetry, **10**, 433–440 (1976).

[15] Sajkiewicz P., Phillips P. J.: Peroxide crosslinking of linear low-density Polyethylenes with homogeneous distribution of short chain branching. Journal of Polymer Science, Part A: Polymer Chemistry, **33**, 853–862 (1995).

[16] Hoffmann M.: Der Einfluß von Verhakungen auf das Dehnungsverhalten von vernetzten Polymeren. Kolloid-Zeitschrift und Zeitschrift für Polymere, **250**, 197–206 (1972).

[17] Heinrich G., Straube E., Helmis G.: Molekularstatistische Theorien polymerer Netzwerke. Fortschrittsbericht. Acta Polymerica, **31**, 275–286 (1980).

[18] Treloar L. R. G.: The physics of rubber elasticity. Oxford University Press, New York (2005).

[19] Smedberg A., Hjertberg T., Gustafsson B.: Effect of molecular structure and topology on network formation in peroxide crosslinked polyethylene. Polymer, **44**, 3395–3405 (2003).

[20] Androsch R., Wunderlich B.: A study of annealing of poly(ethylene-co-octene) by temperature-modulated and standard differential scanning calorimetry. Macromolecules, **32**, 7238–7246 (1999).

[21] Shin K., Nam B. U., Bang J., Jho J. Y.: Melt-state miscibility of poly(ethylene-co-1-octene) and linear polyethylene. Journal of Applied Polymer Science, **107**, 2584–2587 (2008).